




Research Article

Removal of Safranin-T and Toluidine from Water through Gum Arabic/Acrylamide Hydrogel

Salma Jabeen,¹ Sultan Alam,¹ Luqman Ali Shah,² Muhammad Zahoor ,³
Najeeb Ur Rahman,¹ Farhat Ali Khan,⁴ Riaz Ullah ,⁵ Essam A. Ali,⁶
H. C. Ananda Murthy ,⁷ and Aamir Sohail⁸

¹Department of Chemistry, University of Malakand, Chakdara Dir Lower, KPK 18800, Pakistan

²National Center of Excellence in Physical Chemistry (NCE), University of Peshawar, Pakistan

³Department of Biochemistry, University of Malakand, Chakdara Dir Lower, KPK 18800, Pakistan

⁴Department of Pharmacy, Shaheed Benazir Bhutto University, Sheringal Dir Upper, Pakistan

⁵Department of Pharmacognosy, College of Pharmacy, King Saud University, Riyadh, Saudi Arabia

⁶Department of Pharmaceutical Chemistry, College of Pharmacy, King Saud University, Riyadh, Saudi Arabia

⁷Department of Applied Chemistry, School of Applied Natural Science, Adama Science and Technology University, PO Box, 1888 Adama, Ethiopia

⁸MSC Construction Project Management, University of Bolton, UK

Correspondence should be addressed to Muhammad Zahoor; mohammadzahoorus@yahoo.com and H. C. Ananda Murthy; anandkps350@gmail.com

Received 26 February 2022; Accepted 26 April 2022; Published 10 May 2022

Academic Editor: Rabia Rehman

Copyright © 2022 Salma Jabeen et al. This is an open access article distributed under the Creative Commons Attribution License, which permits unrestricted use, distribution, and reproduction in any medium, provided the original work is properly cited.

Hydrogels as “smart sorbents” for wastewater treatment have attracted much attention due to their facile fabrication, rapid regeneration, environment friendly nature, and strong interaction with pollutants. In this study, gum arabic/acrylamide (GA/AM) hydrogel was developed via the free radical polymerization method by employing acrylamide (AM) (monomer), gum arabic (GA) (grafting backbone), N,N-methylenebisacrylamide (MBA) (chemical crosslinker), and tetramethylethylenediamine (TEMED) (accelerator). The fabricated adsorbent was characterized by scanning electron microscopy (SEM), Fourier transform infrared (FTIR) spectroscopy, and surface area analyzer. The adsorption properties of the subject hydrogel were explored against cationic safranin and toluidine dyes in aqueous media. The point of zero charge (PZC) for the GA/AM sorbent was found to be $pH_{PZC} = 7.1$ whereas maximum sorption occurred at pH 11. Different kinetic and isotherm models were applied to evaluate the adsorption mechanism and estimate values of different adsorption parameters. The adsorption isotherm and kinetics were better explained by the Langmuir isotherm and pseudo-second-order kinetic model whereas the adsorption thermodynamics depicted the endothermic, spontaneous, and favorable nature of the process. The adsorbent was regenerated with acetone and reused for the selected dyes for many cycles. After the 5th cycle, the hydrogel retained safranin/toluidine removal capacity $\geq 60\%$ which pointed toward the reusability of the prepared adsorbent for cycles without appreciable reduction in its adsorption capacity. Hence, the GA/AM sorbent can be applied as an alternative of activated carbon to treat dye-contaminated waters.

1. Introduction

Different industries such as textile [1], paint [2], food [3], and pharmaceuticals [4] are the direct emitters of different pollutants [5] including dyes [6] and heavy metal ions

[7, 8] into water. The presence of these toxic pollutants can cause severe environmental problems that can adversely affect the biotic components of the ecosystem as well [9, 10]. Apart from it, they also affect the human health by causing problems such as skin irritation, cancer, and allergic

dermatitis [11]. Therefore, it is important to remove dyes from contaminated water before their discharge into main sewerage lines.

Currently, numerous techniques are in use for the reclamation of dye-contaminated water which are broadly classified into physical, chemical, and biological methods. Among them, the most frequently used techniques are degradation, ion exchange, coagulation, oxidation, photocatalysis, and adsorption [12–14]. Out of them, adsorption is the best and most efficient technique used for the dye's removal from wastewater due to its low cost, reasonably greater efficiency, and easy availability. A large number of materials have been tested as adsorbents (like zeolites, activated carbon, and synthetic polymers) for the removal of dyes and heavy metals from water. It has been observed that hydrogels have exhibited superior efficiencies towards the adsorptive removal of various dyes and inorganic pollutants [15–19]. The cross-linked polymeric networks of hydrogel make it a superior material which can imbibe a lot of water inside its network. The swelling behavior and active charges on the hydrogel network are responsible for dyes and other pollutant's effective removal from contaminated water. Therefore, the hydrogel modifications require a key consideration to use them in an effective way in water reclamation from contaminants [20, 21]. Superabsorbent polymer hydrogels represent the most important class of the polymeric hydrogels which are porous and have an immensely crosslinked three-dimensional skeleton. Simple preparation, easy separation, high efficiency, and low cost are some of the distinctive properties of these hydrogels. These hydrogels have the unique ability to bind or dissolve water hundred times more than other adsorbents because of their hydrophilicity and swelling potential [22, 23]. Gum arabic is a high-molecular weight natural polysaccharide obtained from the tree of *Acacia*. It is composed of 1,3-linked β -D-galactopyranosyl units. The side chains are made of two to five 1,3-related β -D-galactopyranosyl units, combined with the core chain by 1,6-connections. Both the side and the core chains contain units of α -L-arabinofuranos, α -L-rhamnopyranosyl, β -D-glucopyranosyl, and 4-O-methyl- β -D-glucopyranosyl [24, 25]. According to recent literature, the gum Arabic nanohydrogel and polyacrylamide (PAM) nanohydrogel have been fabricated by the microwave-assisted technique. Such hydrogels have been used as adsorbent for removal of crystal violet dye from water [26]. Similarly, GA/poly (acrylic acid) hydrogel has been developed and applied as adsorbent for the removal of methylene blue dye from wastewater [27]. Another study about the fabrication of GA/poly(acrylamide)/Ni(OH)₂/FeOOH hydrogel and its subsequent use as adsorbent for the dye removal from wastewater has also been reported [28]. Moreover, hydrogel synthesized from *gum arabic*, polyacrylate, and polyacrylamide has also been documented in literature which has displayed good adsorption properties toward eradication of methylene blue from wastewater [29]. So far, the use gum arabic/acrylamide hydrogel for adsorption of safranin and toluidine has not been documented in literature which promoted us to fabricate and apply gum arabic/acrylamide hydrogel for adsorption of the mentioned cationic dyes.

In this study, the gum arabic/acrylamide (GA/AM) hydrogel was fabricated from gum arabic and acrylamide in the presence of N, N-methylenebisacrylamide (MBA) (chemical cross-linker) and tetra-methyl ethylene diamine (TEMED) (accelerator). The fabricated adsorbent was used for the removal of safranin and toluidine stains/dyes from water. Since the dyes have received a plethora of applications in industries like paper, textile, and silk, the dyes are also used as redox initiators and photosensitizers and for staining cell organelles. Despite their numerous applications, there are meagre reports regarding their removal from wastewater by using hydrogels which promoted us to utilize safranin and toluidine as model pollutants in the present study.

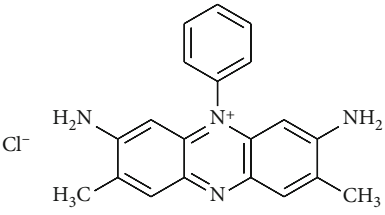
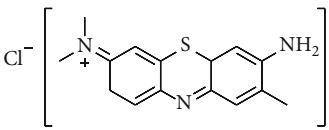
2. Materials and Method

2.1. Chemicals. All the chemicals used in the experiments were of analytical grade and were used without further purification. Safranin and toluidine dyes/stains were purchased from Sigma-Aldrich (Germany). The physicochemical properties of the selected dyes are given in Table 1. Other chemicals used in this study include acrylamide (AM) ($\text{CH}_2=\text{CHC}(\text{O})\text{NH}_2$) obtained from FLUKA (Switzerland), gum arabic (GA) ($\text{C}_{15}\text{H}_{20}\text{NNaO}_4$) obtained from Merck (USA), N-N-methylenebisacrylamide (MBA) bought from FLUKA (Switzerland), and ammonium persulphate (APS, $\text{NH}_4)_2\text{S}_2\text{O}_8$ from FLUKA (Switzerland) used as an initiator while tetramethylethylenediamine (TEMED) was obtained from FLUKA Switzerland.

2.2. Instrumentation. The prepared hydrogel (GA/AM) was characterized by scanning electron microscopy (SEM) (JSM5910, JEOL Tokyo, Japan). The surface area of the hydrogel was determined by Quantachrome (NOVA2200e, Quantachrome, Boynton Beach, Florida, USA) while the functionalities on the surface of the adsorbent were determined using Fourier transform infrared spectroscopy (FTIR) (Thermo Fisher Nicoletis50). The sample in form of a KBr pellet was scanned from 4000 to 500 cm^{-1} . The dye concentration was determined calorimetrically by measuring absorbance using a double-beam ultraviolet-visible (UV-vis) spectrophotometer (UV-1800, Shimadzu Scientific Instruments Inc., Kyoto, Japan) at a specified wavelength mentioned in Table 1. All the adsorption experiments were conducted in the thermostated water bath shaker.

2.3. Synthesis of Polymeric Hydrogel. The polymeric sorbent was prepared using a free radical polymerization approach in which AM was used as a monomer and GA as the backbone onto which the acrylamide chains were grafted. Briefly, 1 gram each of AM and GA was charged to 200 mL water in a beaker followed by stirring the mixture (500 rpm) at 333 K which resulted into the formation of a homogenous mixture. Dropwise 20 μL tetramethyl ethylene diamine (TEMED) was then added followed by 5% ammonium persulphate (APS) solution. This resulted into the development of polymeric GA/AM hydrogel which was washed with water and dried for 420 min in an oven at 338 K. Finally, the dried hydrogel (GA/AM) was grinded

TABLE 1: Physiochemical properties of safranin and toluidine dyes [48, 49].

Name of dye	Safranin T	Toluidine blue
Chemical formula		
Molecular formula	C ₂₀ H ₁₉ N ₄ + Cl ⁻	C ₁₅ H ₁₆ ClN ₃ S
Molecular weight	350.85 g/mol	270.374 g/mol
λ max	554 nm	625 nm
Water solubility	0.05 g/mL	38.2 g/100 mL
Solubility in other solvents	Soluble in alcohol	Slightly soluble in alcohol: ethanol, methanol

with a hammer-type minigrinder and stored till the commencement of adsorption experiments.

2.4. Point of Zero Charge of the Prepared Adsorbent. Point zero charge abbreviated as PZC is the characteristic pH value at which the surface charge of a material becomes zero, i.e., all its active sites are neutral. The PZC of the GA/AM hydrogel was calculated by placing 0.01 g hydrogel in 30 mL of 0.1 N NaNO₃ solution. Each solution was divided in 11 bottles having different pH ranges from 2 to 11, monitored by a pH meter (Ph-2106). The pH of solutions was adjusted by 0.1 M NaOH and 0.1 M HNO₃ solution. The bottles were then kept in a shaker 24 h. The resultant final pH of the bottles was noted where the difference in pH values of the sample was calculated using the equation $\Delta\text{pH} = \text{pH}_i - \text{pH}_f$ [30] with pH_i denoting the initial pH and pH_f the final pH of the given solution.

2.5. Adsorption Experiments. The adsorption performance of prepared adsorbent towards safranin and toluidine dyes in aqueous solution was measured using the batch experimental approach, such as 0.01 g polymeric hydrogel which was stirred with 10 mL dye solution in distilled water (0.001 M). In the kinetic study, a series of reagent bottles containing the same volume (10 mL) and concentration 0.001 M of selected dyes were mixed with 0.01 g of prepared adsorbent and then shaken on a thermostated shaker for 30 min at 293, 313, and 333 K. A specified volume of the sample was filtered and analyzed by a UV-visible spectrophotometer at 554 and 625 nm, respectively, for the remaining concentration of safranin and toluidine. All the experiments were performed in triplicate. Different kinetics models (given in equations (1) to (4)) were used to explain the kinetics of the adsorption process [31].

The pseudo-1st-order equation is expressed as equation (1) as follows:

$$\log (q_e - q_t) = \log q_e - \frac{k_1 t}{2.303}. \quad (1)$$

The pseudo-2nd-order equation is expressed as equation (2) as follows:

$$\frac{t}{q_t} = \frac{t}{q_e} + \frac{1}{k_2 q_e^2}. \quad (2)$$

The Elovich equation is expressed as equation (3) as follows:

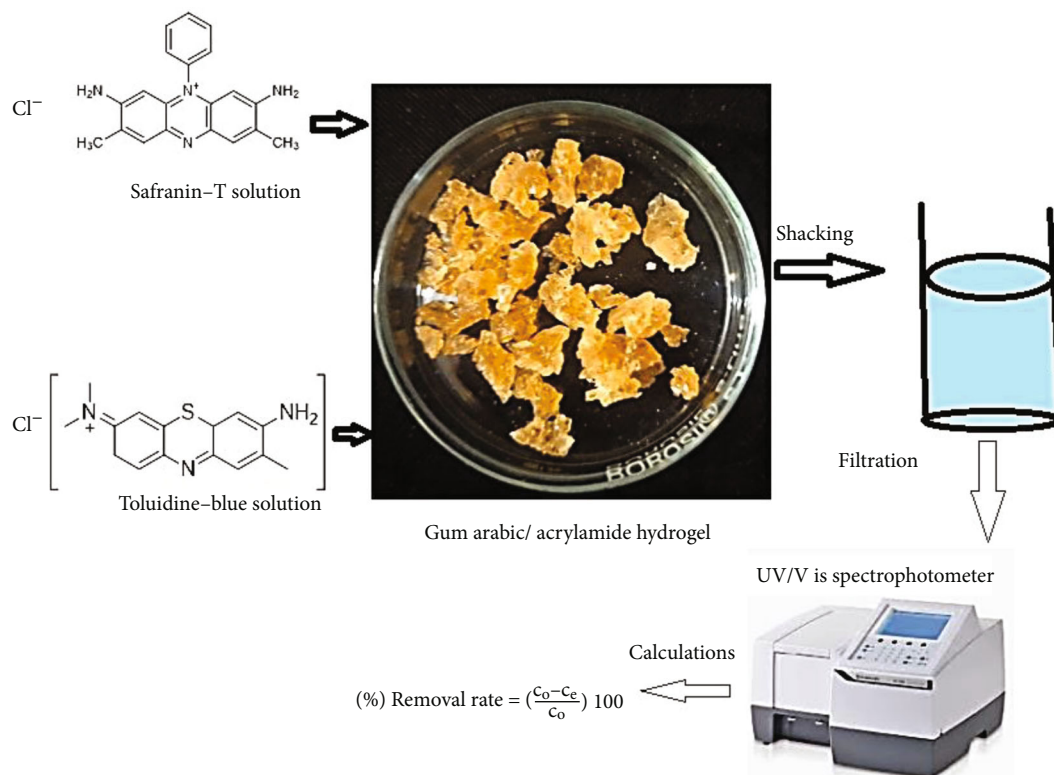
$$q_t = \ln \frac{\beta \alpha}{\alpha} + \frac{\ln t}{\beta}. \quad (3)$$

The intraparticle diffusion model is expressed as equation (4) as follows:

$$q_t = K_i t^{1/2} + C. \quad (4)$$

In these equations, q_e and q_t are the adsorption capacities at equilibrium and at any time t in mol/g, k_1 is the rate constant of the pseudo-1st-order model (1/min), k_2 is the rate constant of the pseudo-2nd-order equation (g/mg/min), α is the initial adsorption rate (mg/g-min), β is the desorption constant (mg/g-min), and C is the intercept in equation (4) whereas, k_{id} is the intraparticle diffusion constant (mg/g-min^{1/2}).

In the isotherm studies, a series of reagent bottles containing 10 mL of different concentrations (0.0005–0.003) of selected dyes were mixed with 0.01 g of the prepared adsorbent and then shaken on a thermostated shaker for 30 min at 293, 313, and 333 K. Specific amounts of sample were filtered and analyzed for the remaining concentration of selected dyes using a UV-visible spectrophotometer. For the determination of different isotherm parameters, Langmuir, Freundlich, and Temkin models were used. Such types of studies are important to evaluate how the adsorbate interacts with the adsorbent and also gives information about adsorption capacities. Isotherm parameters also give information on the formation of a monolayer or multilayer over the adsorbent surface by the adsorbate [32, 33].



SCHEME 1: Schematic representation of the adsorption process.

The Langmuir isotherm model defines the sorption of adsorbate at homogenous sites on the adsorbent surface where the adsorbate only forms a monolayer on the surface of the adsorbent. The linear form of this model can be given as equation (5) as follows:

$$\frac{C_o}{C} = \frac{C_e}{c_{\infty}} + \frac{1}{K_{ad} C_{\infty}}, \quad (5)$$

where C , C_o , K_{ad} , and C_{∞} are the adsorbed amount of dye at equilibrium (mg/g), the concentration of dye solution at equilibrium (mg/L), Langmuir constant (L/mol), and the maximum adsorption capacity (mg/g), respectively, [34].

The Freundlich isotherm model describes the nonideal behavior and reversibility of the adsorption process being nonrestricted to the monolayer formation which can be applied to the adsorption on heterogeneous surfaces (multi-layer adsorption) with nonuniform distribution of adsorption heat and affinities of the sites over the adsorbent surface. Mathematically, this model can be given as equation (6) as follows:

$$\ln q_e = \ln K_f + \frac{1}{n} \ln C_e, \quad (6)$$

where q_e , C_e , K_f , and $1/n$ represent the quantity of adsorbate adsorbed at equilibrium, the equilibrium concentration of dye solution, adsorption capacity at unit concentration, and adsorption intensity. It should be noted that if $1/n = 0$, the adsorption process will be irreversible while favorable

when $0 < 1/n < 1$ and, if $1/n > 1$, the process will be unfavorable [35].

The Temkin model in the linear form can be given as equation (7) as follows:

$$q_e + B_1 \ln k_T + B_1 \ln C_e, \quad (7)$$

where B_1 and K_T are the constant of adsorption and equilibrium binding, respectively [36].

The whole process carried out can be represented as follows (Scheme 1):

Furthermore, the effect of pH on adsorption was investigated using a series of reagent bottles at different pH ranging from 3 to 11 in which pH values were adjusted using dilute solutions of HCl or NaOH ($0.1 \text{ mol}\cdot\text{L}^{-1}$); then, the same volume and concentration of selected dyes were mixed with 0.01 g of the prepared hydrogel and shaken on a thermostatic shaker for 60 min.

The effect of temperature on the selected dye adsorption was evaluated at 293, 313, and 333 K where the same concentration solutions were contacted with the fixed amount of adsorbent for 60 min. The Van't Hoff plot was drawn to estimate values of enthalpy and entropy changes whereas Gibbs free energy values were estimated from the enthalpy and entropy values at respective temperatures.

The polymeric hydrogel was recycled for 5 cycles where the dye-loaded hydrogel was washed with acetone using the solvent extraction method. The recycled hydrogel was dried in an oven at 373 K and reused for 5 cycles to estimate the reduction in adsorption capacity values and consequently the possibility of regeneration of hydrogel.

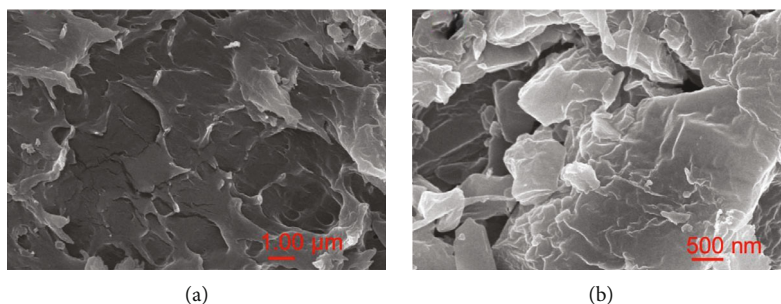


FIGURE 1: SEM images of hydrogel at various magnifications: (a) 1.00 μm and (b) 500 nm.

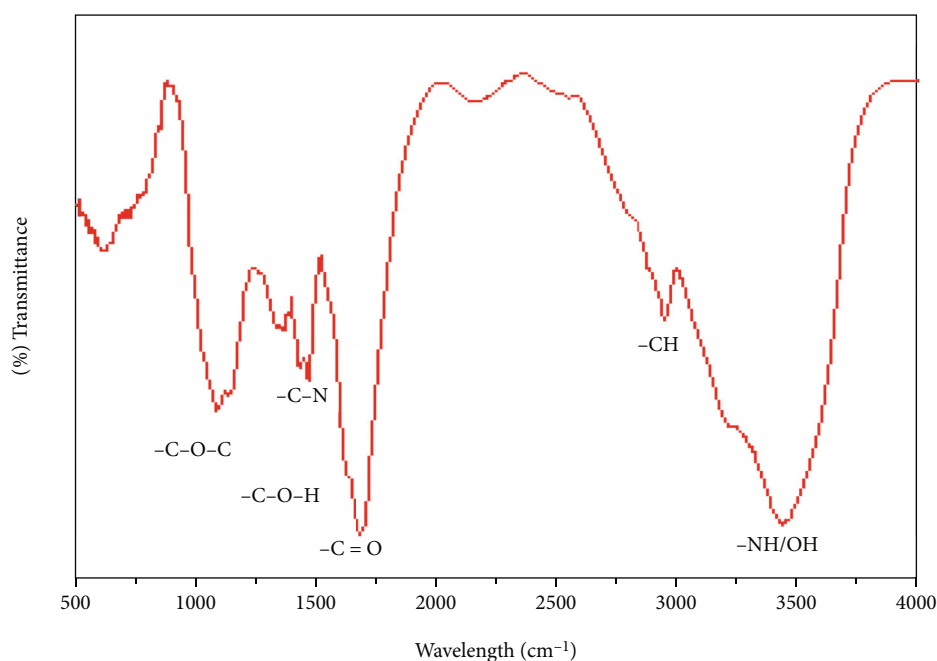


FIGURE 2: FTIR spectrum of polymeric GA/AM hydrogel.

3. Results and Discussion

3.1. Surface Morphology. The morphology of polymer hydrogel was studied using SEM analysis. The SEM images are shown in Figure 1. The micrographs show rough interfaces along with many cavities with characteristic irregular channels of hydrogel that would probably be responsible for the enhanced adsorption of the selected dyes [26, 28].

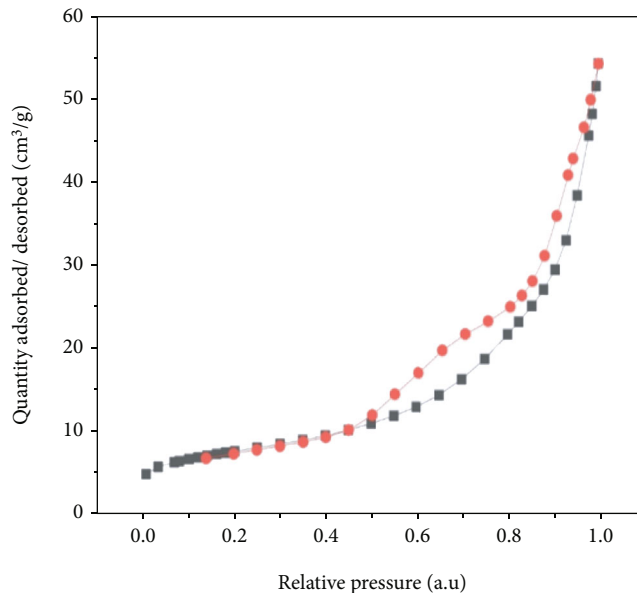
3.2. Surface Functionalities. FTIR spectroscopy was used to identify the surface functional groups on polymeric hydrogel as shown in Figure 2. Both characteristic bands of the acrylamide and gum arabic are present in the synthesized hydrogel. The broad and strong peak at 3428 cm^{-1} is related to the NH or OH stretching of the carboxylic and hydroxyl groups of acrylamide [26, 28, 29]. The medium peaks at $1067\text{--}1090\text{ cm}^{-1}$ represent the stretching vibration of C–O–C and C–O–H bonds. The sharpest peak at 1669 cm^{-1} is related to C=O stretching. The amide bond presence was confirmed from a weak and obvious band at 1456 cm^{-1} ,

which is due to the C–N bending vibration. The two strong peaks at $1565\text{--}1648\text{ cm}^{-1}$ shows the C=O stretching [37, 38]. The presence of peaks for both of hydrogel and acrylamide in FTIR spectra confirm the formation of the polymeric hydrogel network that was attempted to be prepared through a free radical polymerization reaction in this study.

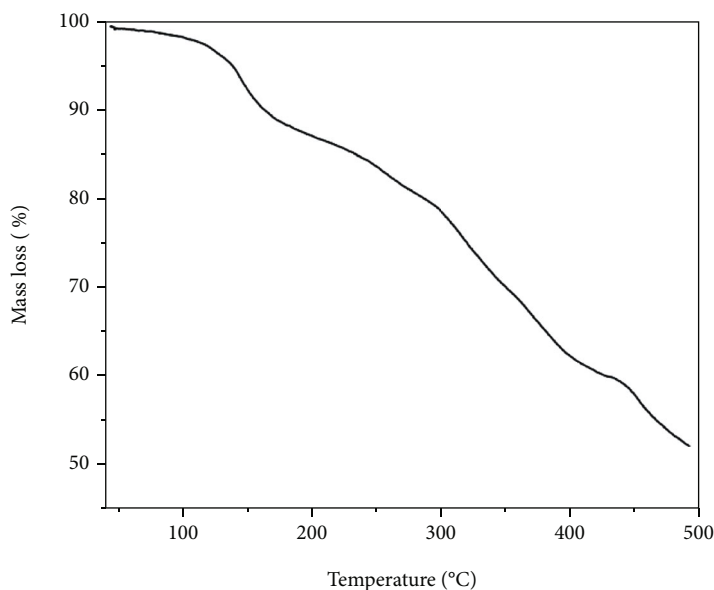
3.3. Surface Area and Thermal Properties of the Hydrogel. Various models like Brunauer-Emmett-Teller (BET), Brookhurst Junior High (BJH), Langmuir, and Dubinin-Radushkevitch (DR) are used to find out the surface area of the adsorbents. Among the abovementioned methods, the commonly used method is BET surface area (m^2/g) analysis that is frequently used to determine the specific surface area, pore size, and pore distribution of the adsorbents. This method involves the nitrogen adsorption and desorption processes (Table 2). The isotherm of the adsorption-desorption of hydrogel refers to the type IV isotherm as shown in Figure 3. The increase in pore size distribution can be confirmed from increase in area under the hysteresis

TABLE 2: Surface area and pore size distribution of hydrogel GA/AM.

Surface area (m ² /g)	Pore size distribution				
	BJH methods		DR method		
BET	Pore volume (cm ³ /g)	Pore diameter (Å)	Micropore volume (cm ³ /g)	Average pore width (Å)	Ads. Energy (kJ/mol)
26.7350	0.068	10.453	0.068	11.179	3.853



(a)



(b)

FIGURE 3: Characterization of hydrogel: (a) BET surface area and (b) thermogram.

loops with increase in temperature. The BET equation is expressed as equation (8) as follows [39].

$$\frac{1}{W(P_0/P) - 1} = \frac{1}{WmC} + \frac{C-1}{WmC} \left(\frac{P}{P_0}\right), \quad (8)$$

where W is the weight of gas adsorbed, P/P_0 is relative pressure, W_m is the weight of adsorbate constituting a monolayer coverage, and C is related to the energy of adsorption in the first adsorbed layer.

The thermogram of GA/AM sorption as presented in Figure 3(b) displays three phases of mass loss corresponding

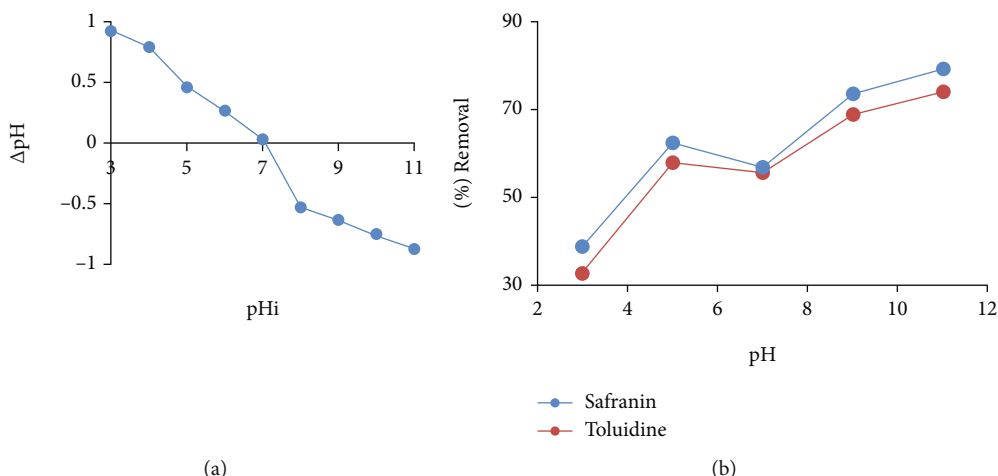


FIGURE 4: (a) Point of zero charge (conditions: temp 313 K, dose 0.01–0.005, time 24 h, pH range (2–11) adjusted by 0.1 M HNO₃ and NaOH, using NaNO₃ 0.1 N solution and volume 30 mL) and (b) effect of pH on the % removal of safranin and toluidine by hydrogel.

to different temperature domains. The first phase with 5% (40–130°C) mass loss is due to the elimination of water molecules and dehydration of neighboring –COOH functionalities [40, 41]. The second (130–250°C) mass loss can be attributed to decarboxylation of the remaining –COOH groups. The final-phase (250–500°C) mass loss is most probably due to the degradation of polymeric chains and breakage of the 3D polymeric network of the hydrogel.

3.4. Point of Zero Charge (PZC) and pH Effect on the Absorption of Safranin and Toluidine. The PZC of GA/AM was noted as 7.1 in Figure 4(a). The surface was positively charged at acidic pH whereas at basic pH, it was negatively charged. As both the dyes are cationic, therefore, the favorable interaction was observed at 11 pH and high adsorption was observed at this pH as shown in Figure 4(b).

The process of adsorption of the dyes (safranin, toluidine) from the solution by superabsorbent hydrogel takes place under the influence of two types of driving forces in which the first one is diffusion of dyes in the network of hydrogel that occurs whereas the second deriving force is electrostatic interactions between adsorbent and adsorbate. The pH of media markedly affects the process of adsorption [26, 28, 29]. Figure 4(b) explains the effect of pH on the selected dye adsorption. The rate of adsorption increases with the increase in pH of the medium. At PZC, the percentage removal of dyes decreases slightly as the isoelectric point is lying there. The percentage removal then abruptly increases after PZC as the pores became negatively charged; thus, maximum adsorption of the dyes occurred [26, 28, 29]. The hydrogel showed a %removal of 78 to 73 for safranin and toluidine at highest pH tested whereas the % removal was 56 and 55% for safranin toluidine, respectively, at PZC (pH 7.08). The % removal of the selected dyes was calculated using equation (9).

$$\% \text{removal} = \frac{C_0 - C_e}{C_0} \times 100. \quad (9)$$

3.5. Effect of Contact Time on Adsorption. The effect of contact time on the absorption of dyes, safranin and toluidine, was investigated in the abovementioned fed-batch experiment described in detail. The results are graphically shown in Figures 5 and 6 for safranin and toluidine, respectively. Initially, the rate of adsorption is high as there is no competition for adsorption sites being free. Up to 60 min, the rate of adsorption increases proportionately, and then, equilibrium is reached where adsorption and desorption rates are equal; thus, the curve has become parallel up to 480 min. The adsorption rate in the beginning is high because of the availability of a larger number of active sites on the surface of hydrogel. Such types of behavior have been observed in other studies as well [42]. Thus, 60 min time was noted as equilibrium time for the 0.01 g hydrogel used.

3.6. Adsorption Kinetics. Adsorption kinetics are important while evaluating the adsorption processes, and one can get insight into the adsorption mechanism and adsorbate-adsorbent interaction [43]. From an economical point of view in the industries, it is important to have information about kinetics of a given process.

The experimental data of the kinetics study were fitted into different models which are graphically shown in Figures 7(a)–7(d) (safranin) and Figures 8(a)–8(d) (toluidine). The slope and intercept values in the case of each model were calculated and interpreted as valuable adsorption parameters listed in Tables 3(a) and 3(b). The R^2 (linear correlation coefficients) values (0.99) of pseudo-second-order plots (Figures 7(b) and 8(b)) are significantly higher than that of pseudo-first-order plots (Figures 7(a) and 8(a); $R^2 = 0.82$ – 0.96) indicating the chemical nature of the sorption process [44, 45]. Also, the Q_e experimental and calculated values in the case of the pseudo-second-order model are close to each other, clearly indicating that the best fit of the kinetics data can be achieved with this model. Moreover, the k_2 values increase with the rise in temperature which indicates a high adsorption rate at elevated temperature.

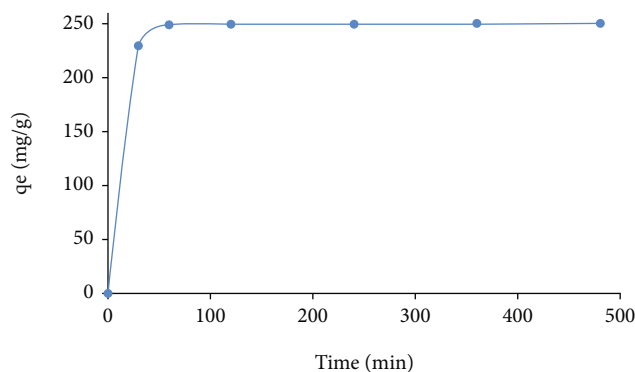


FIGURE 5: Effect of time on the adsorption of safranin on polymeric hydrogel (adsorbent dosage 0.01 g, dye solution 10 mL, time 30–480 min, pH = 11, temperature 313 K).

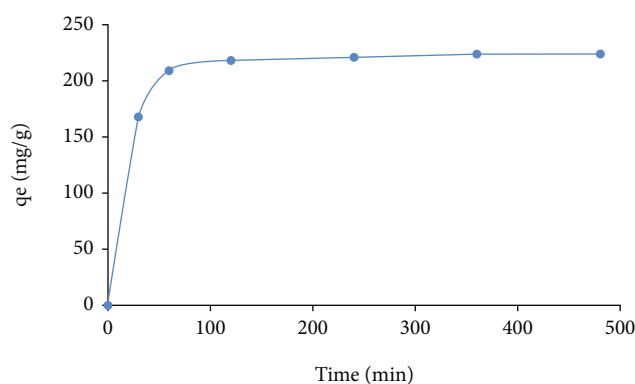


FIGURE 6: Effect of time on the adsorption of toluidine on polymeric hydrogel (adsorbent dosage 0.01 g, dye solution 10 mL, time 30–480 min, pH = 11, temperature 313 K).

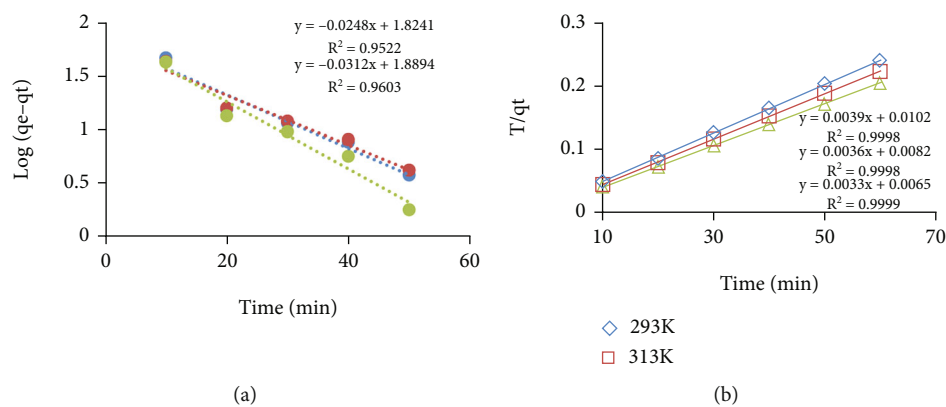


FIGURE 7: Kinetics of safranin adsorption on GA/AM (adsorbent 0.01, dye solution 10 mL, pH 11, temp 313 K, time 60 min): (a) pseudo-1st-order plot and (b) pseudo-2nd-order plot.

The R^2 values of the intraparticle diffusion plots depicted in Figure 1(a) (safranin) and Figure S2a (toluidine) are less than those of Elovich plots displayed in Figure S1b (safranin) and Figure S2b (toluidine). Thus, the Elovich model appropriately describes the data where electrostatic bond formation between the cationic sites of safranin/toluidine and anionic carboxylate groups of the hydrogel is predominant [46].

3.7. Isotherm Studies. To determine the surface properties and affinity of the adsorbent towards various environmental contaminants, various isotherm models like Langmuir, Freundlich, and Temkin models were used. Their theoretical and mathematical backgrounds have been described in the experimental section. The estimated parameters calculated are described as follows:

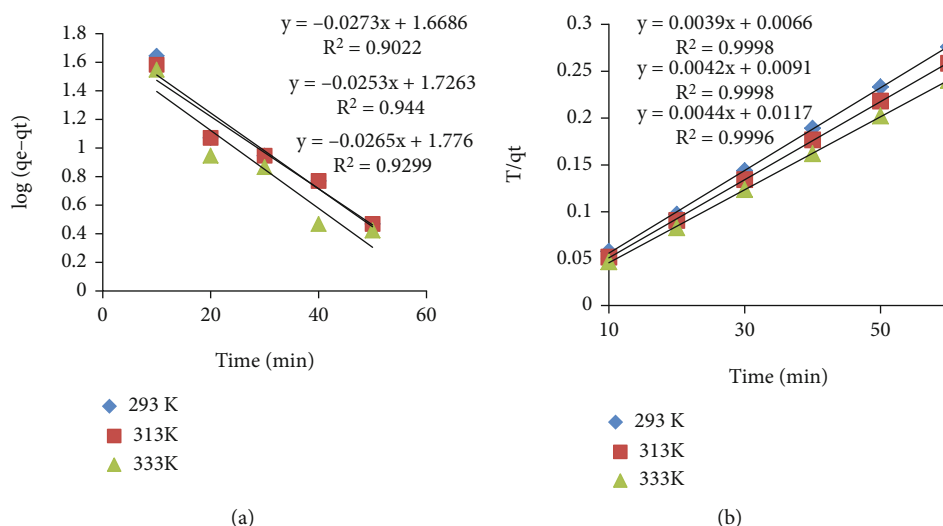


FIGURE 8: Kinetics of toluidine adsorption on the GA/AM (adsorbent 0.01, dye solution 10 mL, pH 11, temp 313 K, time 60 min): (a) pseudo-1st-order plot and (b) pseudo-2nd-order plot.

TABLE 3

(a) Kinetics parameters estimated from the kinetics model for safranin adsorption on the prepared adsorbent

Parameter	293 K	313 K	333 K
Pseudofirst order			
K_1 (min^{-1})	0.57	0.053	0.072
Q_e (mg/g; calculated)	66.69	61.03	77.52
Q_e (mg/g; experimental)	249	268	295
R^2	0.9522	0.9572	0.9603
Pseudosecond order			
Q_e (mg/g; calculated)	256.4	277.7	303.1
Q_e (mg/g; experimental)	249	268	295
K_2 (g/mg/min)	1.49×10^{-3}	1.59×10^{-3}	1.67×10^{-3}
R^2	0.9998	0.9998	0.9999

(b) Kinetics parameters estimated from the kinetics model for toluidine adsorption on the prepared adsorbent

Parameter	293 K	313 K	333 K
Pseudofirst order			
K_1 (min^{-1})	0.061	0.058	0.063
Q_e (mg/g; calculated)	59.71	53.25	46.62
Q_e (mg/g; experimental)	217.4	232.12	249.77
R^2	0.9299	0.944	0.9022
Pseudosecond order			
Q_e (mg/g; calculated)	227.27	238.09	256.41
Q_e (mg/g; experimental)	217.4	232.12	249.77
K_2 (g/mg/min)	0.00165	0.00194	0.00231
R^2	0.9996	0.9998	0.9998

The Langmuir isotherm plots, C_e/q_e versus C_e , are given in Figures 9(a)–9(c) for safranin and Figures 10(a)–10(c) for toluidine. From the slope and intercept of these plots, the values of K_L and Q_m were estimated. The values of these

constants along with the correlation coefficient R^2 are given in Tables 4(a) and 4(b).

The Freundlich isotherm plots, $\ln q_e$ versus C_e , are shown in Figures 9(d)–9(f) (safranin) and Figures 10(d)–

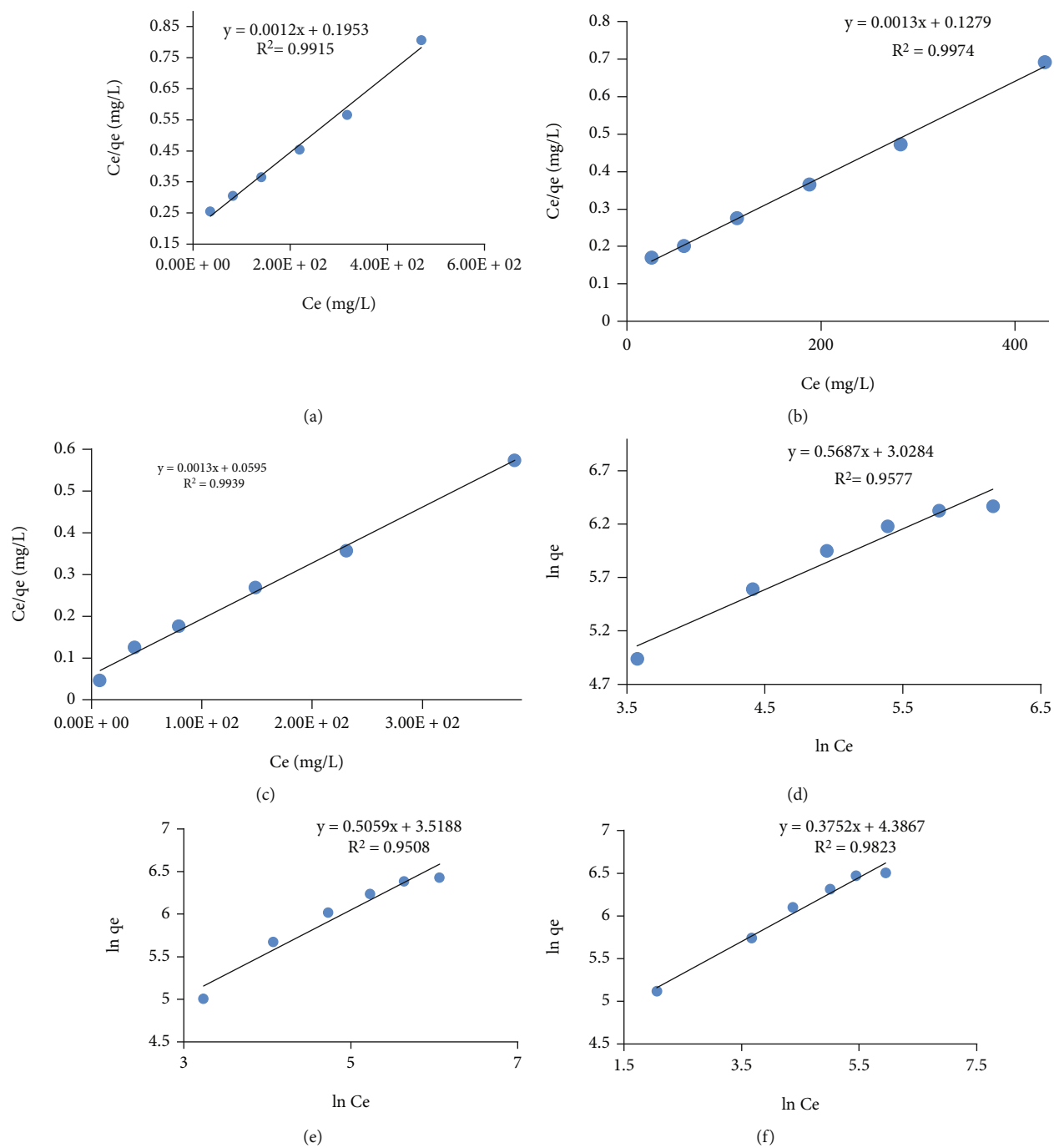


FIGURE 9: Continued.

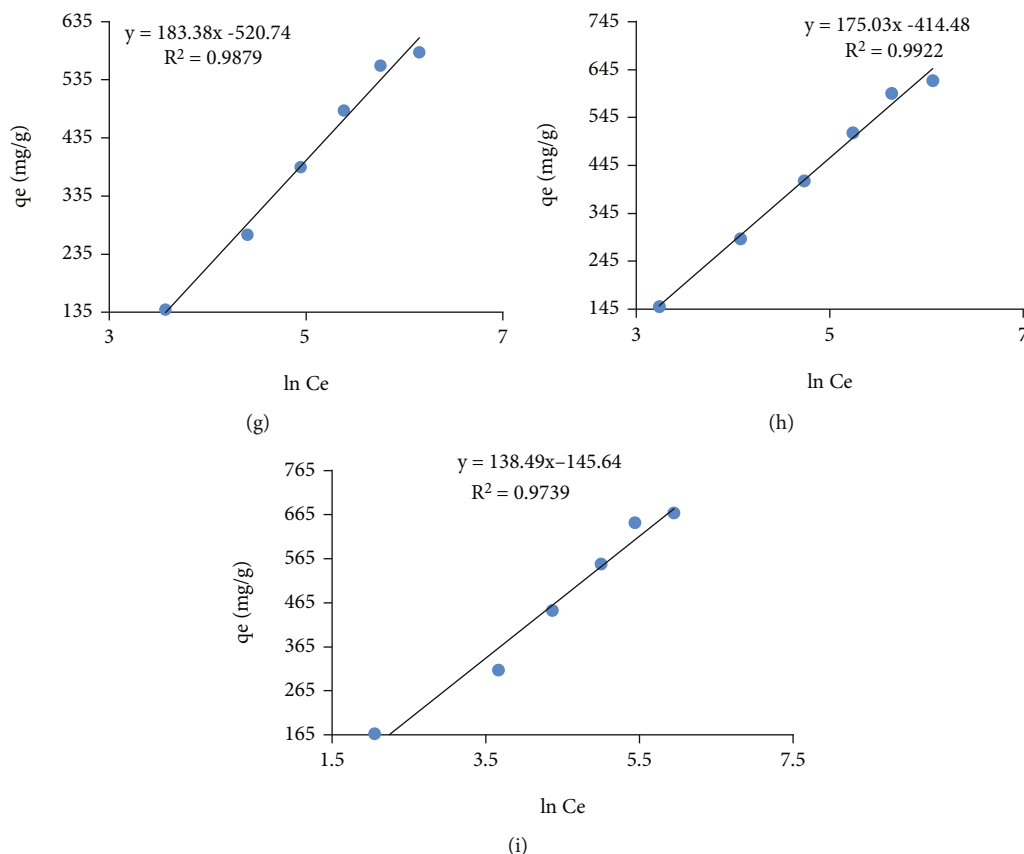


FIGURE 9: Adsorption isotherms for safranin adsorption on the GA/AM (adsorbent 0.01 g, time 60 min, dye solution 10 mL, pH 11, temp 293,313, 333 K). Langmuir isotherm at (a) 293 K, (b) 313 K, and (c) 333 K; Freundlich isotherm at (d) 293 K, (e) 313 K, and (f) 333 K; and Temkin isotherm at (g) 293 K, (h) 313 K, and (i) 333 K.

10(f) (toluidine). Drawing such plots makes it possible to estimate values of constants: n and K_f (from the slope and intercept).

The Temkin isotherm plots, q_e versus $\ln C_e$, that give us the values of the constants of the model are shown in Figures 9(g)–9(i) (for safranin) and Figures 10(g)–10(i) (for toluidine) while the respective values of the constants are shown in Tables 4(a) and 4(b). According to Tables 4(a) and 4(b), the regression values are higher for the Freundlich as compared with those of the Langmuir and Temkin models.

3.8. Thermodynamics of the Process. The thermodynamic parameters for the adsorption of dyes on the polymeric hydrogel were calculated using the following equations (10) and (11):

$$\Delta G^\circ = -RT \ln K_d, \quad (10)$$

where $K_d = q_e/C_e$,

$$\ln \ln(K_d) = \frac{\Delta S^\circ}{R} - \frac{\Delta H^\circ}{RT}. \quad (11)$$

In these equations, ΔG° , ΔH° , and ΔS° are the changes in the Gibbs free energy, enthalpy, and entropy, respectively. A

plot $\ln K_d$ versus $1/T$ defines the parameters: ΔH° and ΔS° that are usually obtained from the slope and intercept of the given plot (Figures 11 and 12). Their values are given in Table 5(a) (safranin) and Table 5(b) (toluidine). The values of Gibbs free energy (ΔG°) were negative at all temperatures indicating a spontaneous nature and feasibility of the process at high temperature. The observed increase in ΔG° values with an increase in temperature suggests that a higher temperature would result in the faster absorption of the dye. The positive value of the ΔH° indicates the endothermic nature of the process and the positive value of entropy show the increase in randomness at the dye/adsorbent interfaces. [47]

3.9. Compression of Adsorption Capacity of Prepared Hydrogel with Those Reported in Literature. The adsorption capacity of the present adsorbent under study was compared with the adsorbent reported in literature as given in Table 6. Despite of the polymeric nature, the hydrogel has exhibited high adsorption capacity as compared with few of those adsorbents reported in literature.

3.10. Reusability and Regeneration of Polymeric Hydrogel. The beauty of the prepared hydrogel adsorbent is reusing by a simple and easy method to remove the entrapped dyes in the hydrogel network structure via the solvent extraction

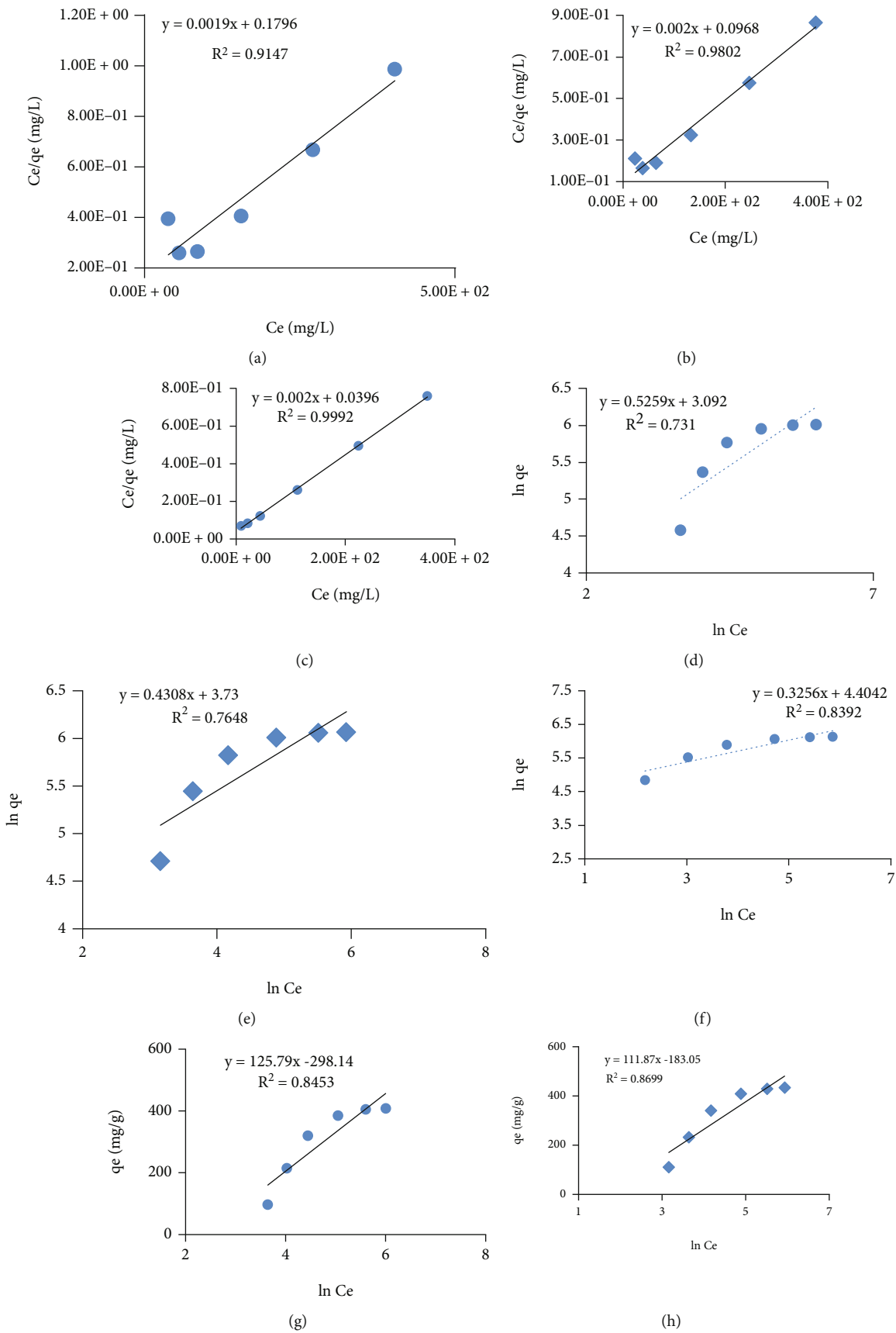


FIGURE 10: Continued.

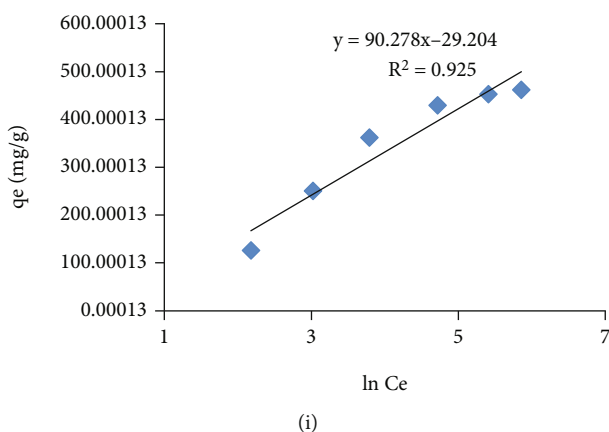


FIGURE 10: Adsorption isotherms for the toluidine adsorption on the GA/AM (adsorbent 0.01 g, dye solution 10 mL, time 60 min, pH 11, temp 293, 313, 333 K). Langmuir isotherm at (a) 293 K, (b) 313 K, and (c) 333 K; Freundlich isotherm at (d) 293 K, (e) 313 K, and (f) 333 K; and Temkin isotherm at (g) 293 K, (h) 313 K, and (i) 333 K.

TABLE 4

(a) Isothermal parameters for the adsorption of safranin dye on the prepared adsorbent

Parameter	293 K	313 K	333 K
Langmuir isotherm model			
Q_m (mg/g)	833	769	769
K_a	6.14×10^{-3}	0.01	0.02
R^2	0.9915	0.9974	0.9939
Freundlich isotherm model			
$1/n$	0.5687	0.5059	0.3752
K_f	20.65	33.72	80.31
R^2	0.9577	0.9508	0.9823
Temkin isotherm model			
B_1	183.38	175.03	138.49
K_T	0.058	0.094	0.349
R^2	0.9879	0.9922	0.9739

(b) Isothermal parameters for the adsorption of toluidine dye on the prepared adsorbent

Parameter	293 K	313 K	333 K
Langmuir isotherm model			
Q_m (mg/g)	526	500	592
K_a	0.0106	0.021	0.051
R^2	0.9147	0.9802	0.9992
Freundlich isotherm model			
$1/n$	0.5259	0.4308	0.3256
K_f	22.1	41.65	81.73
R^2	0.731	0.7648	0.8392
Temkin isotherm model			
B_1	125.79	111.87	90.278
K_T	0.094	0.195	0.724
R^2	0.8453	0.8699	0.925

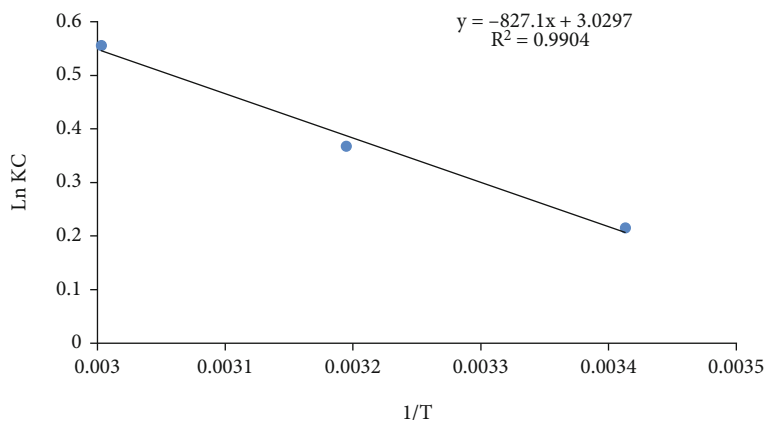


FIGURE 11: Effect of temperature on adsorption of safranin on GA/AM (adsorbent 0.01, dye solution 10 mL, time 60 min, pH 11, temp 293, 313, 333 K).

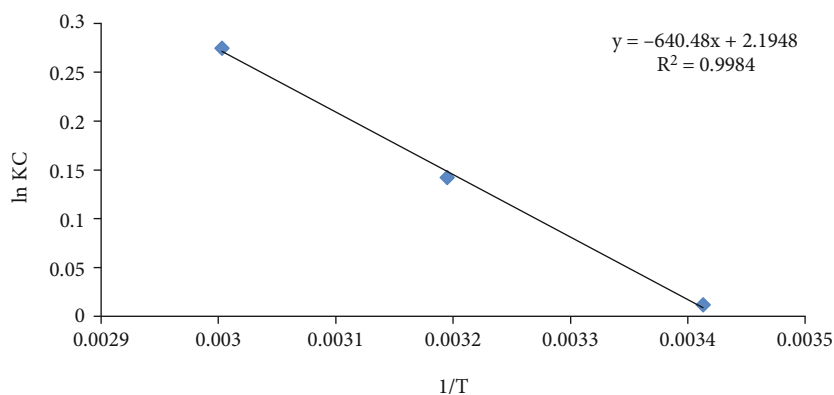


FIGURE 12: Effect of temperature on adsorption of toluidine on GA/AM (adsorbent 0.01, dye solution 10 mL, pH 11, time 60 min, temp 293, 313, 333 K).

TABLE 5

(a) Thermodynamic parameters for the adsorption of safranin on polymeric hydrogel

ΔG° (kJ·mol ⁻¹)			ΔH° (kJ·mol ⁻¹)	ΔS° (kJ·mol ⁻¹ ·K ⁻¹)
293 K	313 K	333 K	6876.51	25.189
-503.845	-1007.647	-1511.427		

(b) Thermodynamic parameters for the adsorption of toluidine on polymeric hydrogel

ΔG° (kJ·mol ⁻¹)			ΔH° (kJ·mol ⁻¹)	ΔS° (kJ·mol ⁻¹ ·K ⁻¹)
293 K	313 K	333 K	5324.951	18.247
-21.42	-386.36	-751.3		

TABLE 6: Comparison of the hydrogel adsorption capacity with the activated carbon adsorption capacity.

S. no.	Adsorbent	Adsorption capacity	References
1	Wood of <i>Paulownia tomentosa</i>	238.44 (mg/g)	[10]
2	Pd-Ni/AC	333.3 (mg/g)	[15]
3	Magnetic activated carbon	149.2 (mg/g)	[21]
4	Activated <i>Ailanthus altissima</i> sawdust	11.46 (mg/g)	[50]
5	Hydrogel gum arabic/acrylamide	526 (mg/g) for toluidine and 833 (mg/g) for safranin	Present study

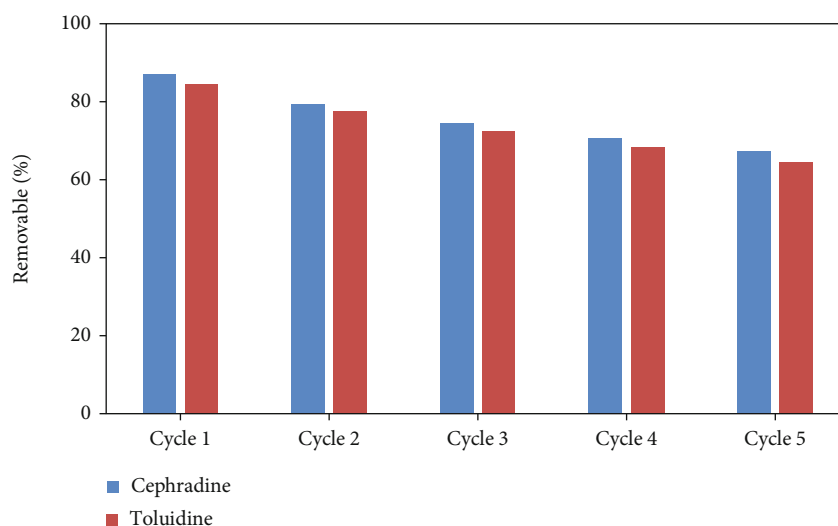


FIGURE 13: Reusability and regeneration of polymeric hydrogel (GA/AM) toward safranin and toluidine dyes.

method. This method is good as compared with others because the dye molecules do not decompose in this method and are recycled its initial state. The regeneration experiment of the hydrogel was investigated in 5 cycles, and the results are as shown in Figure 13 [44, 45].

4. Conclusions

In this study, polymeric hydrogel GA/AM (that has not been used as adsorbent for the selected dyes previously) was prepared by grafting acrylamide on gum arabic with a crosslinker and initiator. The surface morphology and physicochemical properties of the prepared hydrogel were studied by the SEM, FTIR, and BET surface area analyzer. The point of zero charge was also determined in order to explain the effect of pH on the adsorption of selected dyes. Electrostatic interactions between the negatively charged adsorbent surface and positively charged at pH 11 are the responsible factor for high absorption values at the mentioned pH. The adsorption capacities of the prepared adsorbent were 833 mgg^{-1} and 526 mgg^{-1} for safranin and toluidine, respectively, showing that the adsorbent is quite efficient in removing the selected dyes. The adsorption phenomena and kinetics were better explained by the Langmuir isotherm and pseudo-second-order kinetic model whereas the thermodynamic aspects of the adsorption process were endothermic, spontaneous, and favorable at high temperature. After the 5th cycle, an appreciable dye removal ability of more than 60% was still retained showing the reusability of the prepared adsorbent for many times. From the results, it can be concluded that this hydrogel can be used as an alternative of activated carbon to treat water contaminated with toxic dyes.

Data Availability

No data is associated with this submission.

Disclosure

The funders had no role in the design of the study; in the collection, analyses, or interpretation of data; in the writing of the manuscript, or in the decision to publish the results.

Conflicts of Interest

The authors declare no conflict of interest.

Acknowledgments

Authors wish to thank the researchers supporting project number RSP-2021-45 at King Saud University, Riyadh, Saudi Arabia, for their financial support.

Supplementary Materials

Table S1: kinetic parameters estimated from intraparticle and Elovich models for safranin dye adsorption on the prepared adsorbent. Table S2: kinetic parameters estimated from intraparticle and Elovich models for toluidine dye adsorption on the prepared adsorbent. Figure S1: kinetics of safranin adsorption on AG/AM (adsorbent 0.01, dye solution 10 mL, pH 11, temp 313 K, time 60 min): (a) intraparticle diffusion and (b) Elovich model. Figure S2: kinetics for toluidine adsorption on the AG/AM (adsorbent 0.01, dye solution 10 mL, pH 11, temp 313 K, time 60 min): (a) intraparticle diffusion and (b) Elovich model. Figure S3: Freundlich adsorption isotherms at (a) 293 K, (b) 313 K, and (c) 333 K for safranin adsorption on the AG/AM (adsorbent 0.01 g, time 60 min, dye solution 10 mL, pH 11, temp 293,313, 333 K). Figure S4: Temkin adsorption isotherms at (a) 293 K, (b) 313 K, and (c) 333 K for safranin adsorption on the AG/AM (adsorbent 0.01 g, time 60 min, dye solution 10 mL, pH 11, temp 293,313, 333 K). Figure S5: Freundlich adsorption isotherms at (a) 293 K, (b) 313 K, and (c) 333 K for toluidine adsorption on the AG/AM (adsorbent 0.01 g, time 60 min, dye solution 10 mL, pH 11, temp 293,313,

333 K). Figure S6: Freundlich adsorption isotherms at (a) 293 K, (b) 313 K, and (c) 333 K for toluidine adsorption on the AG/AM (adsorbent 0.01 g, time 60 min, dye solution 10 mL, pH 11, temp 293,313, 333 K). (*Supplementary Materials*)

References

- [1] J. Núñez, M. Yeber, N. Cisternas, R. Thibaut, P. Medina, and C. Carrasco, "Application of electrocoagulation for the efficient pollutants removal to reuse the treated wastewater in the dyeing process of the textile industry," *Journal of Hazardous Materials*, vol. 371, pp. 705–711, 2019.
- [2] G. C. de Oliveira Neto, J. M. F. Correia, P. C. Silvade Oliveira, A. G. Sanches, and W. C. Lucato, "Cleaner production in the textile industry and its relationship to sustainable development goals," *Journal of Cleaner Production*, vol. 228, pp. 1514–1525, 2019.
- [3] T. U. Rehman, S. Bibi, M. Khan et al., "Fabrication of stable superabsorbent hydrogels for successful removal of crystal violet from waste water," *RSC Advances*, vol. 9, no. 68, pp. 40051–40061, 2019.
- [4] A. Ullah, M. Zahoor, W. U. Din et al., "Removal of methylene blue from aqueous solution using black tea wastes: used as efficient adsorbent," *Adsorption Science & Technology*, vol. 2022, Article ID 5713077, 2022.
- [5] M. Zahoor, A. Ullah, S. Alam et al., "Novel magnetite nanocomposites (Fe₃O₄/C) for efficient immobilization of ciprofloxacin from aqueous solutions through adsorption pretreatment and membrane processes," *Water*, vol. 14, p. 724, 2022.
- [6] A. Ullah, M. Zahoor, W. U. Din et al., "Removal of methylene blue from aqueous solution using black tea wastes: used as efficient adsorbent," *Adsorption Science & Technology*, vol. 2022, article 5713077, pp. 1–9, 2022.
- [7] A. U. Khan, M. U. Rehman, M. Zahoor, A. B. Shah, and I. Zekker, "Biodegradation of brown 706 dye by bacterial strain *Pseudomonas aeruginosa*," *Water*, vol. 13, p. 2959, 2021.
- [8] S. Alam, B. Ullah, M. S. Khan et al., "Adsorption kinetics and isotherm study of basic red 5 on synthesized silica monolith particles," *Water*, vol. 13, 2803 pages, 2021.
- [9] S. Alam, L. Khan, L. A. Shah, and N. Rehman, "Synthesis of copolymeric hydrogels of acrylamide and 2-(hydroxyethyl methacrylate) and its use for the adsorption of basic blue 3 dye," *Zeitschrift für Physikalische Chemie*, vol. 235, no. 6, pp. 707–721, 2021.
- [10] S. Alam, M. S. Khan, W. Bibi et al., "Preparation of activated carbon from the wood of *Paulownia tomentosa* as an efficient adsorbent for the removal of acid red 4 and methylene blue present in wastewater," *Water*, vol. 13, no. 11, p. 1453, 2021.
- [11] T. U. Rehman, L. A. Shah, M. Khan, M. Irfan, and N. S. Khat-tak Zwitter, "Ionic superabsorbent polymer hydrogels for efficient and selective removal of organic dyes," *RSC Advances*, vol. 9, no. 32, pp. 18565–18577, 2019.
- [12] R. Rehman, A. Jamil, and F. Alakhras, "Sorptive removal of diamond green dye by acid treated *Punica granatum* peels in eco-friendly way," *International Journal of Phytoremediation*, vol. 24, no. 3, pp. 245–254, 2022.
- [13] R. Dar, W. Rehman, U. Zaheer, J. Shafique, and J. Anwar, "Synthesis and characterization of ZnO-nanocomposites by utilizing *Aloe vera* leaf gel and extract of *Terminalia arjuna* nuts and exploring their antibacterial potency," *Journal of Chemistry*, vol. 2021, Article ID 9448894, 7 pages, 2021.
- [14] D. Gumus and F. Akbal, "Photocatalytic degradation of textile Dye and wastewater," *Water Air and Soil Pollution*, vol. 216, no. 1-4, pp. 117–124, 2011.
- [15] A. Umar, M. S. Khan, S. Alam et al., "Synthesis and characterization of Pd-Ni bimetallic nanoparticles as efficient adsorbent for the removal of acid orange 8 present in wastewater," *Water*, vol. 13, no. 8, p. 1095, 2021.
- [16] M. Zahoor, M. Wahab, S. M. Salman, A. Sohail, E. A. Ali, and R. Ullah, "Removal of doxycycline from water using *Dalbergia sissoo* waste biomass based activated carbon and magnetic oxide/activated bioinorganic nanocomposite in batch adsorption and adsorption/membrane hybrid processes," *Bioinorganic Chemistry and Applications*, vol. 2022, Article ID 2694487, 17 pages, 2022.
- [17] M. Muneeb Ur Rahman Khattak, M. Zahoor, B. Muhammad, F. A. Khan, R. Ullah, and N. M. AbdEl-Salam, "Removal of heavy metals from drinking water by magnetic carbon nanostructures prepared from biomass," *Journal of Nanomaterials*, vol. 2017, Article ID 5670371, 10 pages, 2017.
- [18] M. Zahoor, A. Ullah, and S. Alam, "Removal of enrofloxacin from water through magnetic nanocomposites prepared from pineapple waste biomass," *Surface Engineering and Applied Electrochemistry*, vol. 55, no. 5, pp. 536–547, 2019.
- [19] A. Ullah, M. Zahoor, S. Alam, R. Ullah, A. S. Alqahtani, and H. M. Mahmood, "Separation of levofloxacin from industry effluents using novel magnetic nanocomposite and membranes hybrid processes," *BioMed Research International*, vol. 2019, Article ID 5276841, 13 pages, 2019.
- [20] F. Goncalvesa, L. Boaraoa, J. Ferracaneb, and R. Bragaa, "A comparative evaluation of polymerization stress data obtained with four different mechanical testing systems," *Dental Materials*, vol. 28, no. 6, pp. 680–686, 2012.
- [21] L. A. Shah, M. Sayed, M. Fayaz, I. Bibi, M. Nawaz, and M. Siddiq, "Ag-loaded thermo-sensitive composite microgels for enhanced catalytic reduction of methylene blue," *Environmental Engineering*, vol. 2, no. 1, p. 14, 2017.
- [22] G. Phillips and P. Williams, "Tree exudate gums: natural and versatile food additives and ingredients," *Food Ingredients and Analysis International*, vol. 23, pp. 26–28, 2001.
- [23] A. M. Islam, G. O. Phillips, A. Sljivo, M. J. Snowden, and P. A. Williams, "A review of recent developments on the regulatory, structural and functional aspects of gum arabic," *Food Hydrocolloids*, vol. 11, no. 4, pp. 493–505, 1997.
- [24] S. Desplanques, F. Renou, M. Grisel, and C. Malhiac, "Impact of chemical composition of xanthan and acacia gums on the emulsification and stability of oil-in-water emulsions," *Food Hydrocolloids*, vol. 27, no. 2, pp. 401–410, 2012.
- [25] S. Davoudizadeh, M. Sarsabili, and K. Khezri, "Synthesis and characterization of polystyrene/mesoporous diatomite composites via activators generated by electron transfer for atom transfer radical polymerization," *Progress in Polymer Science*, vol. 231, no. 9, pp. 1543–1558, 2017.
- [26] G. Sharma, A. Kumar, M. Naushad et al., "Fabrication and characterization of gum arabic-_{cl}-poly(acrylamide) nano-hydrogel for effective adsorption of crystal violet dye," *Carbohydrate Polymers*, vol. 202, pp. 444–453, 2018.
- [27] E. M. Abdel-Bary and A. M. Elbedwehy, "Graft copolymerization of polyacrylic acid onto Acacia gum using erythro-sine-thiourea as a visible light photoinitiator: application

- for dye removal,” *Polymer Bulletin*, vol. 75, no. 8, pp. 3325–3340, 2018.
- [28] M. Naushad, G. Sharma, and Z. A. Allothman, “Photodegradation of toxic dye using gum arabic-crosslinked- poly(acrylamide)/Ni(OH)₂/FeOOH nanocomposites hydrogel,” *Journal of Cleaner Production*, vol. 241, article 118263, 2019.
- [29] A. G. Ibrahim, A. M. Elkony, and S. M. El-Bahy, “Methylene blue uptake by gum arabic/acrylic amide/3-allyloxy-2-hydroxy-1-propanesulfonic acid sodium salt semi-IPN hydrogel,” *International Journal of Biological Macromolecules*, vol. 186, pp. 268–277, 2021.
- [30] L. S. Jasim and A. M. Aljeboree, “Removal of heavy metals by using chitosan/ poly (acryl amide-acrylic acid) hydrogels: characterization and kinetic study,” *NeuroQuantology*, vol. 19, no. 2, pp. 31–37, 2021.
- [31] G. Crini, “Kinetic and equilibrium studies on the removal of cationic dyes from aqueous solution by adsorption onto a cyclodextrin polymer,” *Dyes and Pigments*, vol. 77, no. 2, pp. 415–426, 2008.
- [32] W. Cheung, Y. Szeto, and G. McKay, “Intraparticle diffusion processes during acid dye adsorption onto chitosan,” *Biore-source Technology*, vol. 98, no. 15, pp. 2897–2904, 2007.
- [33] L. Largitte and R. Pasquier, “A review of the kinetics adsorption models and their application to the adsorption of lead by an activated carbon,” *Chemical Engineering Research and Design*, vol. 109, pp. 495–504, 2016.
- [34] H. Qiu, L. Lv, B. C. Pan, Q. J. Zhang, W. M. Zhang, and Q. X. Zhang, “Critical review in adsorption kinetic models,” *Journal of Zhejiang University-Science A*, vol. 10, no. 5, pp. 716–724, 2009.
- [35] M. Saxena, N. Sharma, and R. Saxena, “Highly efficient and rapid removal of a toxic dye: adsorption kinetics, isotherm, and mechanism studies on functionalized multiwalled carbon nanotubes,” *Surfaces Interfaces*, vol. 21, pp. 100–639, 2020.
- [36] R. A. Gemeinhart, H. Park, and K. Park, “Pore structure of superporous hydrogels,” *Polymers for Advanced Technologies*, vol. 11, no. 8-12, pp. 617–625, 2000.
- [37] C. A. Ibekwe, G. M. Oyatogun, T. A. Esan, and K. M. Oluwasegun, “Synthesis and characterization of chitosan/gum arabic nanoparticles for bone regeneration,” *American Journal of Materials Science and Engineering*, vol. 5, no. 1, pp. 28–36, 2017.
- [38] M. Sudibandriyo, “A simple technique for surface area determination through supercritical CO₂ adsorption,” *Makara Journal of Technology*, vol. 14, no. 1, pp. 1–6, 2010.
- [39] M. A. El-Bindary, I. M. El-Deen, and A. F. Shoair, “Removal of anionic dye from aqueous solution using magnetic sodium alginate beads,” *Journal of Materials and Environmental Science*, vol. 10, no. 7, pp. 604–617, 2019.
- [40] H. Subhan, S. Alam, L. A. Shah, M. W. Ali, and M. Farooq, “Sodium alginate grafted poly(*N*-vinyl formamide- *co* -acrylic acid)-bentonite clay hybrid hydrogel for sorptive removal of methylene green from wastewater,” *Colloids and Surfaces A: Physicochemical and Engineering Aspects*, vol. 611, p. 125853, 2021.
- [41] H. Subhan, S. Alam, L. A. Shah, N. S. Khattak, and I. Zekker, “Sodium alginate grafted hydrogel for adsorption of methylene green and use of the waste as an adsorbent for the separation of emulsified oil,” *Journal of Water Process Engineering*, vol. 46, no. 5, article 102546, 2022.
- [42] H. Patel and R. T. Vashi, “A study on removal of toluidine blue dye from aqueous solution by adsorption onto Neem leaf powde,” *World Academy of Science, Engineering and Technology*, vol. 70, pp. 831–836, 2010.
- [43] J. Deng, Z. Zhai, Q. Yuan, and G. Li, “Effect of solution pH on adsorption of cefradine by wheat straw and thermodynamic analysis,” *Nature Environment and Pollution Technology*, vol. 18, no. 1, pp. 317–321, 2019.
- [44] H. Zhu, Y. Jia, X. Wu, and H. Wang, “Removal of arsenic from water by supported nano zero-valent iron on activated carbon,” *Journal of Hazardous Materials*, vol. 172, no. 2-3, pp. 1591–1596, 2009.
- [45] S. Arabzadeh, M. Ghaedi, A. Ansari, F. Taghizadeh, and M. Rajabi, “Comparison of nickel oxide and palladium nanoparticle loaded on activated carbon for efficient removal of methylene blue,” *Human & Experimental Toxicology*, vol. 34, no. 2, pp. 153–169, 2015.
- [46] F. C. Wu, R. L. Tseng, and R. S. Juang, “Characteristics of Elovich equation used for the analysis of adsorption kinetics in dye-chitosan systems,” *Chemical Engineering Journal*, vol. 150, no. 2-3, pp. 366–373, 2009.
- [47] A. da Silva, N. Bion, F. Epron et al., “Effect of the type of ceria dopant on the performance of Ni/CeO₂ SOFC anode for ethanol internal reforming,” *Applied Catalysis B: Environmental*, vol. 206, pp. 626–641, 2017.
- [48] H. K. Singh, M. Saquib, M. M. Haque, and M. Muneer, “Heterogeneous photocatalysed decolorization of two selected dye derivatives neutral red and toluidine blue in aqueous suspensions,” *Chemical Engineering Journal*, vol. 136, no. 2-3, pp. 77–81, 2008.
- [49] B. P. Nenavathu, S. Kandula, and S. Verma, “Visible-light-driven photocatalytic degradation of safranin-T dye using functionalized graphene oxide nanosheet (FGS)/ZnO nanocomposites,” *RSC Advances*, vol. 8, no. 35, pp. 19659–19667, 2018.
- [50] I. Ullah, S. Alam, M. S. Khan et al., “Activated *Ailanthus altissima* sawdust as adsorbent for removal of acid yellow 29 from wastewater: kinetics approach,” *Water*, vol. 13, no. 15, p. 2136, 2021.